Journal of Photonic Materials and Technology
2025, Vol. 10, No. 2, pp. 13-24
https://doi.org/10.11648/j.jpmt.20251002.11

Research Article

Green Synthesis of Ga-Doped SnO_2 Nanoparticles: Effects of Ga Doping Concentrations on the Structural and Optical Properties

Bethwel Kiprotich, Peter Waithaka, Sylvia Opiyo, Sharon Kiprotich*

Department of Physical and Biological Science, Murang'a University of Technology, Murang'a, Kenya

Abstract

This study explores the transformative impact of gallium (Ga) doping on the structural and optical properties of tin oxide NPs synthesized using chemical and green method. The nanoparticles were synthesized at different doping concentrations of gallium (Ga-SnO_2). The effects of different dopant concentration on structural and optical properties of *Psidium guajava* capped SnO_2 nanoparticles were investigated using X-ray diffraction (XRD), Ultra Violet- Visible spectrophotometer (UV-Vis), Fourier transform infrared and photoluminescence spectroscopy (PL). The bandgap energies of Ga-SnO_2NPs were estimated using Tauc's plot. The bandgap energies were observed to decrease with introduction of gallium. Highest bandgap was obtained at 2.5% and 2.0% Ga-SnO_2NPs having a bandgap value of 3.25 and 3.07 eV for capped and uncapped Ga-SnO_2 respectively. Smallest bandgap was obtained at 0.5% Ga-SnO_2 NPs having a bandgap value of 2.29 and 2.46 eV for capped and uncapped Ga-SnO_2 respectively. Fourier transform infrared spectroscopy showed the stretching vibration of SnO_2 between 690–790 cm^{-1} wavenumbers. Structural analysis using X-ray diffraction (XRD revealed Ga doping significantly leads to a decrease in crystallite size calculated using Scherrer equation. The results obtained showed that both capped and uncapped Ga-SnO_2 maintained the tetragonal rutile structure. This showed that the dopant occupied the interstitial site of the precursor materials. Derby Scherrer formula was used to calculate the crystallite size, the results obtained showed that capping agents and doping reduces the crystallite size of nanoparticles. All nanoparticles formed were in the range of 10.99–18.00 nm. The PL spectrum showed emission at a near band emission and deep level emission.

Keywords

Nanoparticles, Tin Oxide, Band Gap, Green Synthesis, *Psidium Guajava* Extract, Optical Properties

1. Introduction

The Dye-sensitized solar cell (DSSC) photoanode is a promising 3rd generation photovoltaic cell. They are in the limelight for a prospective greener energy source due to their low cost and simple manufacturing method, flexibility, environmentally friendly and comparatively high efficiency of 12.3% [1]. Additional light converters include silicon-based solar cells [2], p-n junctions [3], and hybrid perovskites [4]. Recently, studies have been oriented toward enhancing greener energy conversion by improving DSSCs' main components: the nanocrystal photoanode, dye, counter cathode

*Corresponding author: Skiprotich@mut.ac.ke (Sharon Kiprotich)

Received: 5 September 2025; **Accepted:** 19 September 2025; **Published:** 9 October 2025

Copyright: © The Author(s), 2025. Published by Science Publishing Group. This is an **Open Access** article, distributed under the terms of the Creative Commons Attribution 4.0 License (http://creativecommons.org/licenses/by/4.0/), which permits unrestricted use, distribution and reproduction in any medium, provided the original work is properly cited.

electrode, and electrolyte [5]. However, the efficiency solely lies in the capacity of the photoactive nanocrystal electrode to harvest light and transport photoelectrons that are injected from the photo-excited dye of the semiconductor at the conduction band [6].

For the last three decades, tin oxide (SnO_2) has become one of the most studied semiconductor materials belonging to variety of transparent conductive oxides known as TCOs [7]. The review articles have mostly discussed the challenges and opportunities of indium (In)-doped SnO_2 (ITO). It has both low electrical resistivity and facile pattern ability [8]. However, it lacks temperature stability and resistance to chemical attack. Although the amount of indium is limited in the earth's crust, the human population is prone to its toxicity [9]. The low-rate self-compensation effect makes it more challenging to obtain binary oxide semiconductors having a p-type conductive behavior [10]. These challenges provide an impetus to seek an alternative to ITO, which has high electrical conductivity and comparable visible transmittance.

To solve the challenge, metal doped tin oxide is widely applied for transparent conducting oxide. The advantage of tin dioxide is that it is abundant and non-toxic, has high thermal and chemical stability [11] and UV-resistance properties which make SnO_2 an efficient electron transport layer (ETL) [12], especially in the case of perovskite solar cells. SnO_2 has a wide optical bandgap, 3.6 eV [6] and a high transmittance over the entire visible regime, which indicates that when it is used in an optoelectronic device its absorption losses can be minimized [13]. Earlier studies on SnO_2 reveal that by alloying with metal oxides or doping with metals, its electronic properties can be selectively tuned to obtain a better optoelectronic device performance [14].

Different dopants are used in doping tin oxide which include In [15], Ga [10], Al [16], Sb [17], Zn [18], Cu [19], N [20] used as acceptor dopants. Ga is one of the commonly studied dopants to tailor the electronic properties of SnO_2, as its ionic radius (0.62 Å) is nearly equal to that of Sn^{4+} (0.69Å). Gallium (Ga) doping has been widely investigated for its effects on various semiconductors to enhance their structural, optical, and electronic properties [21]. Different semiconductors, such as lead sulphide (PbS) [22], cadmium oxide (CdO) [23], zinc oxide (ZnO) [24], titanium dioxide (TiO_2) [25], and copper oxide (CuO) [26] have been doped with Ga. Doping with Ga improves key properties such as conductivity, carrier concentration, and optical absorption. High doping concentrations can cause phase separation, forming secondary phases that degrade material quality [27].

Different methods have been used to synthesize SnO_2 nanoparticles such as sol-gel route [28], hydrothermal method [29], spray pyrolysis [30], chemical vapor deposition [31], thermal evaporation of oxide powder [29], and green-method [32]. However, these methods are considered to be harmful to the environment since they utilize toxic reagents and involve tedious procedure to prepare nanoparticles. Therefore, there is need to develop simple and green method to synthesize these nanoparticles. Physical and chemical methods are gradually being replaced by green synthesis methods [33] because of issues related to consumption of large amount of energy [34], release of toxic and harmful chemicals [35] and use of complex equipment and synthesis conditions [36]. Green synthesis provides advancement over chemical and physical methods as it is non-toxic [37], pollution free [33], environment friendly and economical [38].

This method involves the use of plant extract as a capping and stabilizing agent to control the crystal growth of nanoparticles. Flavonoids, terpenoids, phenolics, aldehyde and ketones are the phytochemical components in plant extracts that act as reducing and stabilizing agents. *Psidium guajava* contains abundant amounts of polyphenols which are inexpensive, renewable and widely available and could be efficient for the growth of nanoparticles. Additionally, Psidium guajava extract is simple to obtain and doesn't require costly equipment. The study therefore tries to explore the use of plant extracts in the synthesis of SnO_2 nanoparticles and how various concentration of Ga affects the structural and optical properties of *Psidium guajava* capped SnO_2. The results from the study will give insights on the tunability of the material properties of *Psidium guajava* capped SnO_2 nanoparticles for the targeted solar cell applications.

2. Material and Methods

2.1. Materials

All reagents used were of analytical grade and were used as received: They include stannous chloride dihydrate ($SnCl_2.2H_2O$) (>98%), gallium (III) nitrate hydrate ($Ga(NO_3)_3.XH_2O$) (>99.9%), absolute ethanol (C_2H_5OH) (>99%), guava leaves extract and deionized water. All reagent were purchased from Sigma Adrich & A. B Chem. Deionized water was prepared in Murang'a University of Technology Research Laboratory.

2.2. Preparation of *Psidium Guajava* Leaf Extract

Guava leaves (*Psidium quajava*) were collected from a farm in Murang'a County near Murang'a University of Technology, Kenya. County is located in central Kenya at latitudes of 0 ° 34' S and 1° 7' S and longitudes 36° E and 37°27' E. The samples were first cleaned using running tap water followed by deionized water to remove surface pollutants. The washed leaves were dried in an oven at 50 ℃ for 5 hours before crushing using a blender. 4.0 g of the sample was introduced to 100 ml of deionized water and heated at temperature of 60 ℃ for 30 minutes. After cooling to room temperature, the mixture was filtered using 1 mm Whatman filter paper (Figure 1) [39] and stored in a refrigerator to be used as capping agent in the synthesis.

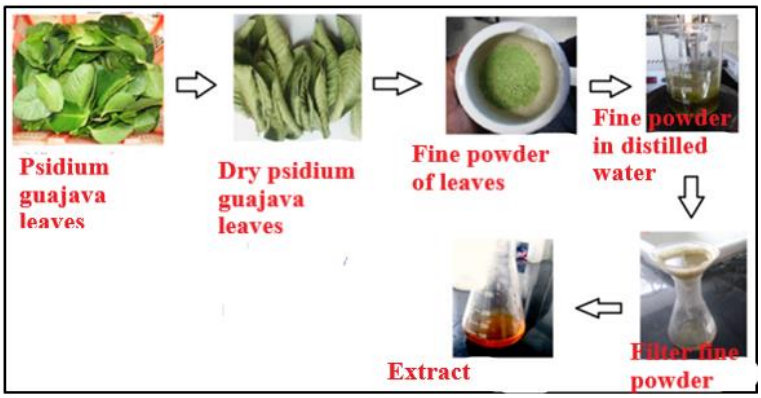


Figure 1. *Schematic representation of Psidium guajava leaves extract preparation.*

2.3. Preparation of Ga Doped SnO_2

Stannous chloride dihydrate with a mass of 1.35 g was dissolved in 30 ml deionized water and stirred for 10 minutes at room temperature. 30 ml of *Psidium guajava* extract (capping agent) was added to the solution after which ammonium hydroxide was added to raise the pH to 9. Different concentration (0.5. 1.0, 1.5, 2.0 and 2.5%) of gallium (III) nitrate hydrate was added and refluxed at 60 ℃ for 3 hours using hot plate. Aging process was allowed for 24 hours after which washing was done using deionized water and absolute ethanol. Drying was done using laboratory oven at 100 ℃ for 2 hours and annealed at 500 ℃ for 3 hours. The process was repeated without *Psidium guajava* extract.

2.4. Characterization Technique

X-ray diffractometer (XRD) model ARL EQUINOX 100 was used at 40 kV, 0.9 mA, with x-rays generated at wavelength of 1.5405 Å at a scanning range of 20°-80° and an interval time of 20 seconds. XRD diffractometer was used to obtain the crystal structure and phase component of the synthesized SnO_2 and Ga-SnO_2 NPs. Photoluminescence spectroscopy (PL) Infitek SPLF97 model was used to determine the electronic structure and defects in nanoparticles. Ultra violet visible spectroscopy (UV-vis) evolution one plus model was used to determine the optical properties of nanoparticles. FTIR model IR Tracer-100 SHIMADZU was used to determine the functional group.

3. Results Discussion

3.1. XRD Analysis

The structural properties of synthesized pure SnO_2 and Ga-SnO_2 NPs were investigated using the XRD diffractometer model EQUINOX 100. Figure 2 depicts the XRD diffraction pattern of synthesized SnO_2 and Ga-SnO_2 NPs capped (a) and uncapped (b) at varying mol% of Ga (0.5, 1.0, 1.5, 2.0 and 2.5%) in 2 θ from 20 °-80 °. The 2 θ value corresponds to the reflection from miller index (110), (101), (200), (211), (220), (002), (310), (301), (202) and (321) which agrees with JCPDS card no 41-1445. Tetragonal rutile structure of SnO_2 was maintained as all diffraction peaks matching well with the standard JCPDS card (41-1445). Uncapped SnO_2 and introduction of Ga shows a growth of a peak at 46 °.

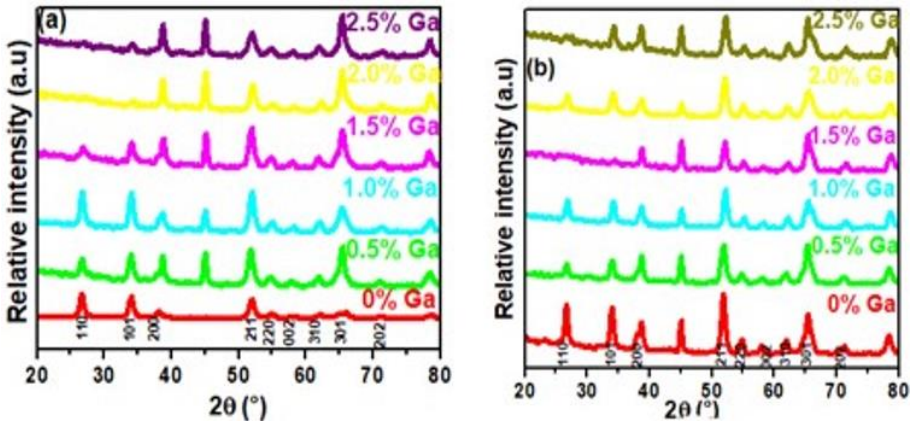


Figure 2. *XRD pattern of synthesized SnO_2 and Ga-SnO_2 with (a) and without (b) Psidium guajava extract in the range 20°-80°.*

The crystallite size of capped and uncapped Ga-SnO_2 was calculated using Scherrer equation (Equation 1) [40].

$$D=\frac{k\lambda}{\beta \cos\theta} \quad (1)$$

Where k is the width constant (0.9), λ is the wavelength which was 1.5406 Å for Cu anode X-ray tube, β is the full width at half maximum (rad) (FWHM) and θ is the Bragg angle. The crystallite size was calculated from the average of four most intense peaks (101), (200), (211) and (301) and table 1 tabulates the results. For uncapped Ga-SnO_2, 2.0% Ga-SnO_2 had the smaller size of 10.99 nm while the highest crystallite size value of 15.23 nm was observed at 2.5%. For capped Ga-SnO_2, 1.5% Ga-SnO_2 has a smaller size of 11.46 nm and a higher crystallite value of 16.27 nm at 0.5% Ga-SnO_2. The decrease in crystallite size when Ga was introduced into SnO_2 indicates that introducing Ga atoms disrupts the natural crystal growth as Ga introduces foreign atoms in SnO_2 as reported by Siyalo *et al* [41]. Since ionic radius of Ga^{3+} is smaller than that of Sn^{4+} and that their substitution or incorporation into the SnO_2 structure creates lattice strain or distortion which inhibits the growth of the crystalline domains, leading to smaller crystallite sizes [42]. Decrease in crystallite size was also reported by Siyalo et al [41] and Shinde et al [43].

The 2θ values represent the diffraction angles in X-ray diffraction (XRD) analysis. Slight shifts in these values indicate changes in the lattice parameters due to doping. For example, addition of Ga to metal oxide caused lattice distortions, leading to shifts in the 2 θ values [44]. The dislocation density (δ), defined as the length of dislocation-lines per unit volume of the crystal was calculated using the equation 2 [45] as table 3 tabulates the results.

$$(\delta) = \frac{1}{D2} \quad (2)$$

Where D is the crystallite size obtained from Scherer equation. The dislocation network within the structure is indicated by the dislocation density and is inversely proportional to crystallite size. For capped Ga-SnO_2, the (δ) value is high at 1.5% with 0.0076 and least at 0.5 with 0.0038. For uncapped sample, the δ value was high at 2.0% with 0.0075 and least at 2.5% with 0.0052. Uncapped and capped Ga-SnO_2 indicates an inverse relationship between the (δ) and crystallite size as shown in figure 3. Change in the interplanar spacing (d) indicates alterations in the crystal structure causing a change in variations indicate changes in the lattice parameters due to Ga incorporation [46]. Stronger nanoparticles with higher dislocation densities and strains have fewer ductile nanomaterials, whereas weaker nanoparticles with lower dislocation densities and strains have more ductile materials.

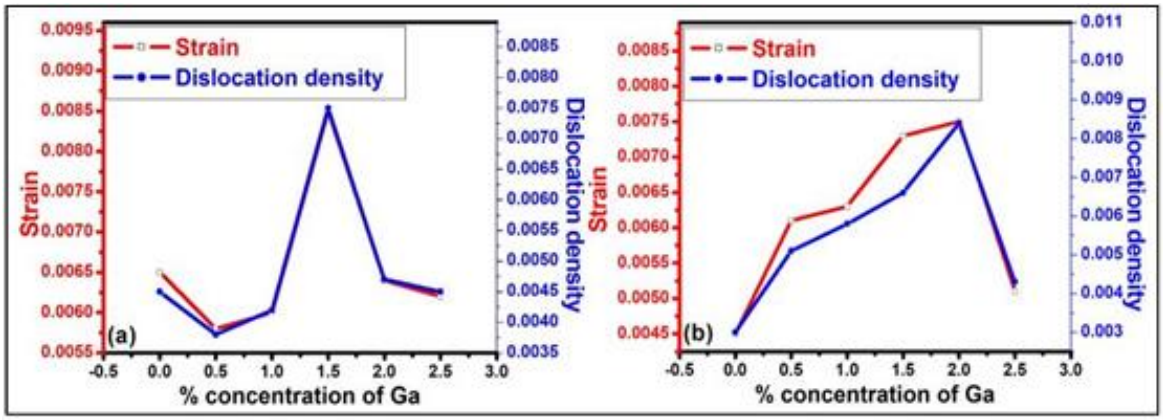


Figure 3. *Trend of micro strain and dislocation density of capped (a) and uncapped (b) Ga-SnO_2.*

Table 1. *2θ, full width at half maximum (FWHM), crystallite size (D) and the dislocation density (δ) for uncapped (a) and capped (b) Ga-SnO_2.*

Materials		Plane	Dopant concentration (%)					
			0%	0.5%	1.0%	1.5%	2.0%	2.5%
Uncapped NPs	2θ	100	26.72	26.76	26.65	26.86	26.82	26.75
		101	34.02	34.02	34.03	34.32	34.18	34.34
		200	38.73	38.34	38.75	38.79	38.68	38.73

Materials		Plane	Dopant concentration (%)					
			0%	0.5%	1.0%	1.5%	2.0%	2.5%
Capped NPs	FWHM	211	51.91	51.91	51.91	52.15	52.12	52.29
		301	65.48	65.41	66.38	65.52	65.55	65.52
		100	0.4985	0.4842	0.9820	0.9674	0.6848	0.9306
		101	0.5318	0.6708	0.5754	1.2718	0.6567	0.5872
		200	0.3521	0.5199	0.5282	0.4585	0.7122	0.4699
		211	0.6089	0.7575	0.7184	0.6447	0.7460	0.6572
		301	0.5257	0.7767	0.9741	0.9415	1.2353	0.6144
	D (av)		18.00	13.10	13.09	12.17	10.99	15.23
	δ		0.0031	0.0052	0.0052	0.0068	0.0083	0.0043
	2θ	100	26.72	26.73	26.90	26.78	26.86	26.70
		101	34.04	34.02	34.06	34.09	34.13	33.98
		200	38.16	38.73	38.72	38.57	38.67	38.71
		211	51.91	51.85	51.95	52.03	52.04	51.85
		301	65.48	65.44	65.42	65.44	65.45	65.43
	FWHM	100	0.5876	0.5985	0.9542	0.5563	0.9454	0.5800
		101	0.6046	0.5329	0.5864	0.5546	0.4308	0.5908
		200	0.6162	0.4653	0.4470	1.0602	0.5217	0.4806
		211	0.7299	0.6725	0.5777	0.6850	0.6094	0.6485
		301	0.4727	0.5177	0.7260	0.9419	1.0307	0.6745
	D (av)		14.89	16.27	15.33	11.46	14.77	14.80
	δ		0.0045	0.0038	0.0043	0.0076	0.0046	0.0046

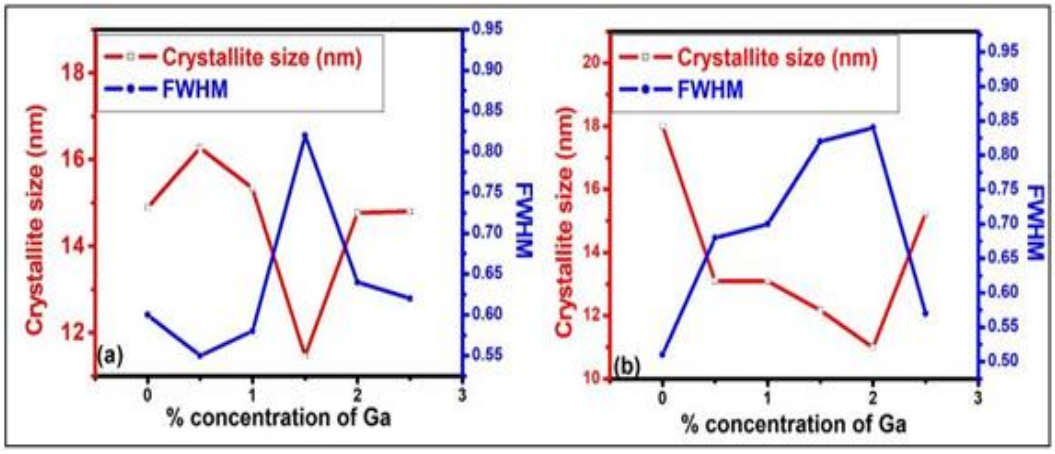


Figure 4. *Relationship between crystallite size and FWHM of capped (a) and uncapped (b) Ga-SnO_2.*

For both capped and uncapped Ga-SnO_2, high intense peaks were observed at (101), (200), (211) and (301). The peaks were broadened with increase in concentration of Ga and which shifted towards high angle. This is because the ionic radius of trivalent Ga^{3+} (0.062 nm) is much smaller than that of Sn^{+4}. An increase in crystallite size is indicated by a de-

crease in FWHM (Figure 4) and macrostrain. Variation in FWHM suggest crystallite size and strain changes due to different doping levels [47]. It is observed that the FWHM is inversely proportional to crystal size: crystal size $\alpha \frac{1}{FWHM}$ [48], the variation was not constant with variation in concentration and a decrease in FWHM generally indicates an increase in crystallite size [28] (Figure 4).

Lattice strain was calculated using equation (3) [47].

$$\in = \frac{\beta}{4 \tan \theta} \quad (3)$$

Figure 5 shows the variation of strain with crystal size, it is observed that crystallite size is inversely proportional to strain [41]. Interstitial doping and nanocrystal size fluctuation were identified as the causes of the strain and lattice parameter variations,,,, Changes in strain were attributed to the incorporation of Ga, which introduced lattice distortions and defects [47] due to slight difference in ionic radius and different oxidation states, contributed to the reduced crystallite size. Nanoparticles with a smaller crystallite size have a larger surface are to volume ratio thus higher surface energy causing higher strain [49].

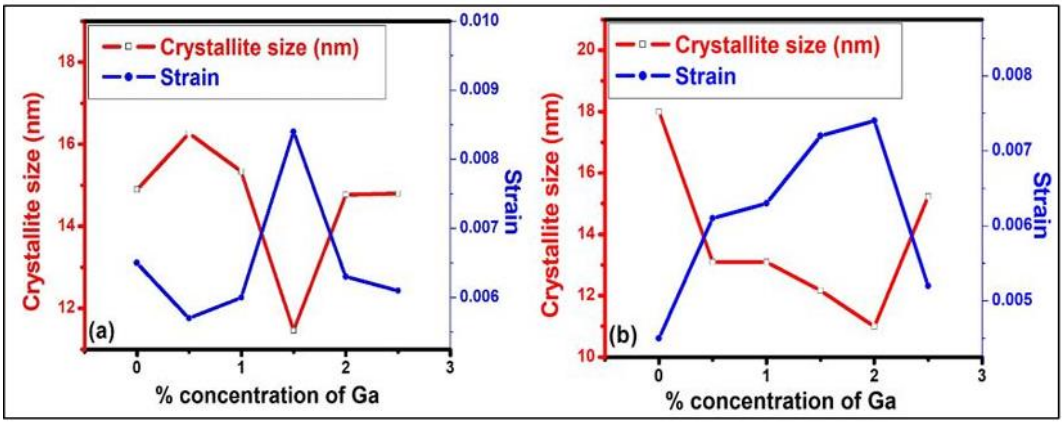


Figure 5. *Shows the variation in crystallite size and strain for capped (a) and uncapped (b) Ga-SnO_2.*

3.2. UV-Vis Analysis

Figure 6 shows the absorption spectra of synthesized SnO_2 and Ga-SnO_2 with (a) and without (b) *psidium guajava* extract at different mol% of gallium. The absorption is related to the bandgap of the material [50]. The highest and the lowest intensity was observed at 2.0% and 0.5% Ga-SnO_2 respectively for the capped NPs while for the uncapped NPs, the highest and the lowest intensity was observed at 2.0% Ga-SnO_2 and pure SnO_2 respectively. Ga doping alters the density of states in the conduction and valence bands as gallium introduces new energy states or altered pre-existing energy levels [44]. Additionally, by modifying defect states, Ga doping can reduce recombination losses, improving charge separation and transport which is a critical factor for the efficiency of solar cells as reported by Siyalo *et al* [44]. The absorption edge of different samples varies as the concentration of Ga in the SnO_2 nanoparticles varies.

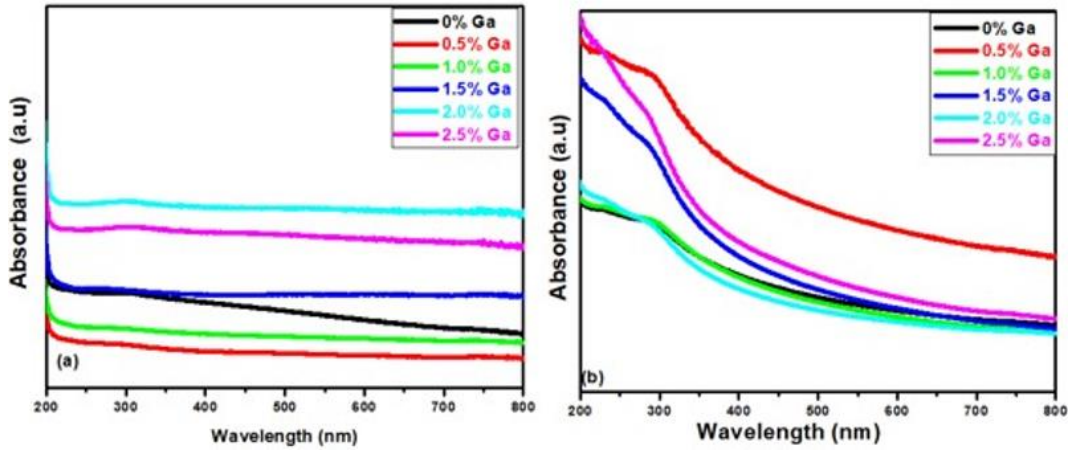


Figure 6. *Absorption spectra of synthesized pure SnO_2 and Ga-SnO_2 with (a) and without (b) the Psidium guajava extract.*

Figure 7 provided shows Tauc's plot for capped (a) and uncapped (b) Ga-SnO_2 at different mol concentration. The analysis involves the determination of the optical bandgap energy using Tauc's relation [24].

$$(\alpha hv)^n=\beta(hv-E_g) \quad (4)$$

Where α is the absorption coefficient, hv is the incident photon energy, β is the proportionality with a value of 1 and E_g is the optical energy band gap. By extrapolating the linear portion of each curve (the rising edge) to the x-axis, the intercept of the linear section of $(\alpha hv)^2$ versus hv plot on the hv axis was used to determine the average energy band gaps as shown in Figure 8 and the values were tabulated in Table 2. This process identifies the photon energy at which electronic transitions occur from the valence band to the conduction band.

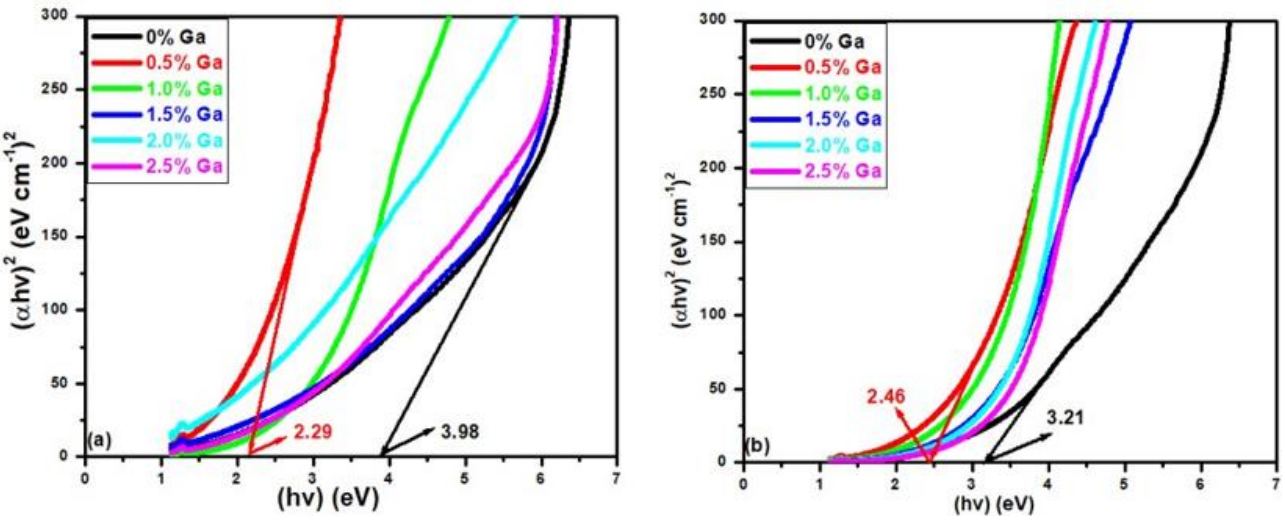


Figure 7. *Tauc's plot estimate of synthesized SnO_2 and Ga-SnO_2 with (a) and without (b) Psidium guajava extract.*

For capped Ga-SnO_2 NPs, the band gap decreases from 3.25 eV to 2.29 eV with 2.5% Ga-SnO_2 having a highest band gap and 0.5% Ga-SnO_2 having the smallest band gap. For uncapped Ga-SnO_2, the band gap decreases with 2.0% and 0.5% Ga-SnO_2 having the highest and smallest band gap respectively. Decrease in bandgap was also reported by Seid et al [52] for Ga doped ZnO. Ga atoms introduce additional energy levels within the bandgap, these energy levels likely arise due to structural defects or changes in the electronic density of states caused by doping, which shifts the absorption edge to higher or lower photon energies, depending on the doping concentration [51]. The newly introduced energy levels may serve as intermediate states, facilitating multi-photon absorption and subsequently improving the efficiency of photocatalysis under visible or near-ultraviolet light.

The decrease in band gap with addition of dopants is due to the shrinkage effect which occurs due to the induced shift of the minimum conduction band and maximum valence band [53]. Even though, the crystallite size and the band gaps expected to be changed oppositely, explanations for such a condition can also be due to the quantum size effect which can cause the shrinkage of the band gaps [54, 55]. The bandgap decreases indicating the substitutional incorporation of Ga^{3+} into the SnO_2 lattice introduces donor states therefore reducing the optical bandgap.

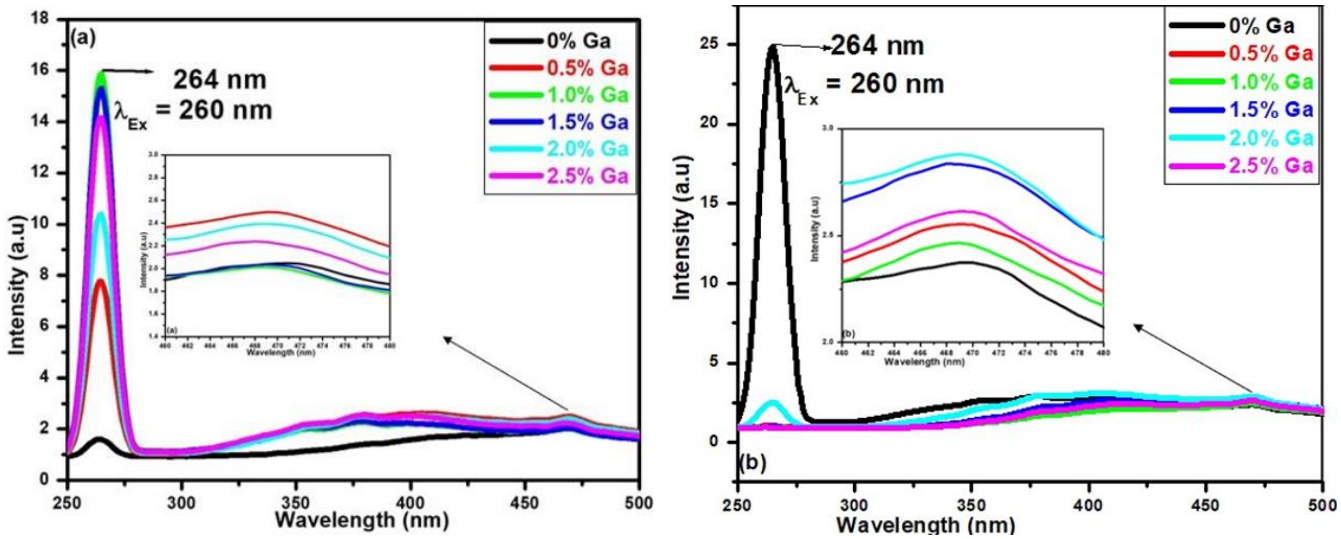
Table 2. *Energy bandgap of pure SnO_2 and Al-SnO_2 synthesized with and without Psidium guajava extract.*

Dopant concentration	Capped (eV)	Uncapped (eV)
Pure SnO_2	3.98	3.21
0.5%	2.29	2.46
1.0%	2.79	2.78
1.5%	3.19	3.0
2.0%	3.17	3.07
2.5%	3.25	2.90

The lower band gap energy helps in increasing number of electron-hole pair. Ga doping tunes the optical bandgap of SnO_2, highlighting its potential for tailoring electronic and optical properties for specific applications, such as photovoltaics. Decrease in the band gap indicates a change in absorption, hence reflecting changes in the material's electronic structure, providing a means to engineer SnO_2 materials with desired optical characteristics.

3.3. Photoluminescence Analysis

Figure 8 depicts room temperature photoluminescence spectra of synthesized pure SnO_2 and Ga-SnO_2 with and without *Psidium guajava* extract respectively. The excitation spectrum has a peak around 264 nm with different peak intensity as shown in figure 8. The absorption peaks suggest that the material absorbs energy causing electrons to move from the valence band to the conduction band, creating excited states. From figure 8 (a), excitation spectra increased when Ga was introduced with 1.0% showing the highest intensity while 0.5% Ga-SnO_2 had a lowest intensity. From Figure 8 (b), pure SnO_2 had the highest intensity and 2.5% Ga-SnO_2 had the lowest intensity.



(a) (b)

Figure 8. *Photoluminescence spectra of synthesized pure and Ga-SnO_2 with (a) and without (b) Psidium guajava extract.*

Photoluminescence spectra show two types of emission: near band edge emission (NBE) in UV region and defect level emission (DLE) in the visible region. The inset in figures 4 and 5 represents the DLE in the range (460 nm – 480 nm) for capped and uncapped Ga-SnO_2 respectively. For SnO_2 and Ga-SnO_2, emission peak was observed at 354.62, 378.74 and 468.21 nm. Peak at 354.62 and 378.74 nm corresponds to the near band edge, are attributed to the radiative recombination of the photoexcited electron in the conduction band with the photo generated hole in the valence band [11, 50]. Emission in the NBE was also reported by Seid et al [52].

Table 3 shows the, peak centre and intensity of Ga-SnO_2 at varying concentration of Ga synthesized with (a) and without (b) *Psidium guajava* extract. For capped Ga-SnO_2, maximum peak intensity was observed at 0.5% with an increment of 0.49 from pure SnO_2. A decrease in intensity was noted at 1.0% and 1.5% Ga-SnO_2 with a decrease of 0.04 and 0.02 respectively. For uncapped Ga-SnO_2, maximum peak intensity was observed at 2.0% with an increment of 0.53 compared to pure SnO_2. Increase intensity in the visible emission for Ga doped samples has been reported by Siyalo et al [51], Asedy *et al* [56] and Shinde et al [43]. Similar red-shift has been observed in the dominant PL peak for other oxide spectra, example, for SnO_2 on doping with Mn [57], for ZnO on doping with Ag [58] visible emission corresponds to the transition of photon energy carriers from donor levels of interstitial atoms to the acceptor vacancy levels [52]. The enhanced intensity is due to the introduction of free carrier concentration (electrons) by gallium and due to the increasing quality of Ga^{3+} acceptors [11]. Also, Ga enhances the radiative recombination process due to introduction of new energy states or localized states within the bandgap that allow more efficient electron transitions [41]. Decrease in the intensity may be attributed to the decreased quantity of radiative transitions of interstitial oxygen by diffusion to oxygen vacancies [59]. Similar observation has been reported by Seid *et al* [52]. Addition of a divalent/trivalent ion in a Sn ion, results in an increase in the number of O-vacancies, producing O-vacancies related traps, which make a strong contribution to the luminescence [60].

Enhanced emission properties due to Ga doping can improve the performance of photo catalytic and other optoelectronic devices, where efficient light emission and controlled luminescence are essential. The enhanced UV emission is indicative of an improvement in crystallinity and was verified by the observable decrease in the DLE peak intensity with the increase in mol%. This is due to the decrease in the concentration of interstitial oxygen in the SnO_2 nanostructures which occurs when Ga is doped in SnO_2. In the process the residual O ions get consumed by Ga^{+3} ions [61]. Doping with Ga enhances light absorption and prolongs the lifetime of photo-generated carriers. This enhancement is essential for photocatalytic processes while the newly introduced energy levels

may serve as intermediate states, facilitating multi-photon absorption and subsequently improving the efficiency of photocatalysis under visible or near-ultraviolet light [41].

Table 3. Peak centre and intensity of Ga-SnO_2 at varying mol concentration of gallium.

Dopant concentration	Capped Ga-SnO_2		Uncapped Ga-SnO_2	
	Peak centre (nm)	Intensity (a. u)	Peak centre (nm)	Intensity (a. u)
0% (Pure SnO_2)	471.12	2.03	470.16	2.31
0.5%	468.71	2.52	468.99	2.58
1.0%	468.74	1.98	468.99	2.46
1.5%	468.50	2.0	468.95	2.80
2.0%	468.87	2.40	468.99	2.84
2.5%	468.90	2.22	468.92	2.62

3.4. FTIR Analysis

FTIR Spectroscopy was used to identify the chemical bonding and functional groups in both capped and uncapped Ga-SnO_2. Figure 9 shows the FTIR spectra in the range 400-4000 cm^1 for capped (a) and uncapped (b) NPs. The stretching of Sn-O for capped and uncapped SnO_2 is responsible for the peaks at 783.42 and 698.21 cm^{-1} respectively. O-H bending, probably from phenolic compounds, is responsible for the peak at 954.09 cm^{-1} for capped SnO_2, whereas O-H bending, most likely from water and hydroxyl groups, is responsible for the peak at 892.33 cm^1 for uncapped Ga-SnO_2. For both capped and uncapped SnO_2, the peak at 1148.69 and 1063.51 is caused by C-O stretch. For capped Ga-SnO_2, the peak is an indicative of alcohol or ester group while the peak at 1389.46 and 1326.39 cm^{-1} for capped and uncapped Ga-SnO_2 is due to C-H bending. Peak at 2982.46 (capped) and 2921.90 cm^{-1} (uncapped) typically indicates C–H stretching vibrations, which can be associated with aliphatic or potentially aromatic groups. The peak at 3662 cm^{-1} (capped) and 3604 cm^{-1} (uncapped) is due to O-H stretching indicative of hydroxyl group.

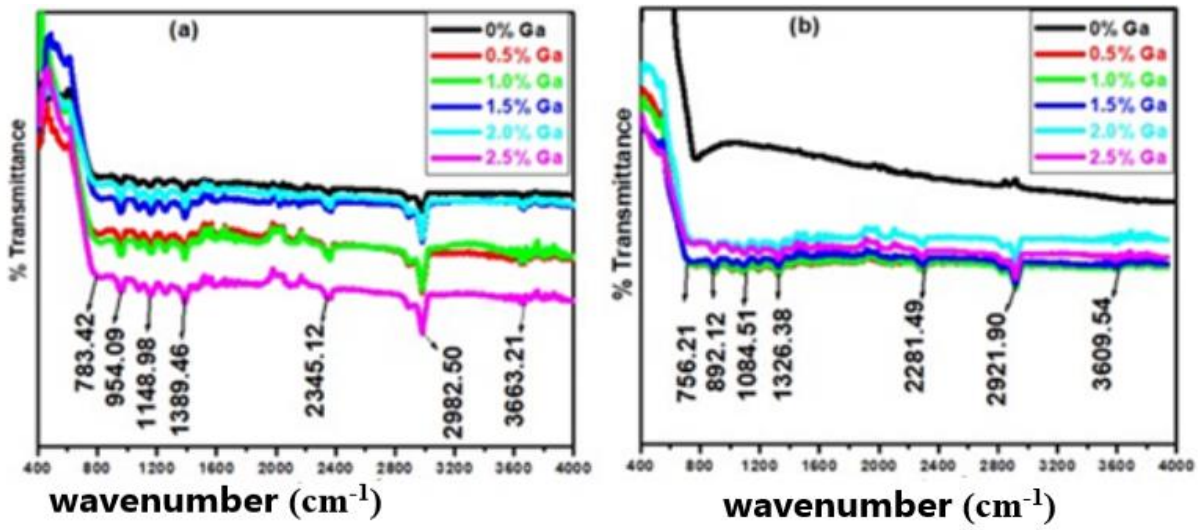


Figure 9. FTIR spectra of capped (a) and uncapped (b) Ga-SnO_2 at varying concentrations of the dopant.

4. Conclusion

The capping agents had major impacts in both structural, morphological and optical properties of nanoparticles. The XRD analysis showed that the tetragonal rutile structured of SnO_2 was maintained. The use of capping agents and Ga doping decreases the particle size. The use of capping agents increases the intensity of the emission band. The band gap of the nanoparticles were lower than that than that of the bulk due to quantum defects.

Abbreviations

DLE	Deep Level Emission
FWHM	Full Width Half Maximum
Ga	Gallium
NBE	Near Band Emission
NPs	Deep Level Emission

Acknowledgments

Special thanks to BMBF, the German Ministry of Education and Research and UNESCO – TWAS for funding the work. The authors also wish to the thank Murang'a University of Technology for providing us with synthesis and characterization equipment's.

Conflicts of Interest

The authors declare no conflicts of interest.

References

[1] A. A. Qureshi *et al.*, "Facile formation of SnO_2–TiO_2 based photoanode and Fe_3O_4@ rGO based counter electrode for efficient dye-sensitized solar cells," *Mater. Sci. Semicond. Process.*, vol. 123, p. 105545, 2021.

[2] M. Okil, M. S. Salem, T. M. Abdolkader, and A. Shaker, "From Crystalline to Low-cost Silicon-based Solar Cells: a Review," *Silicon*, vol. 14, no. 5, pp. 1895–1911, Apr. 2022, https://doi.org/10.1007/s12633-021-01032-4

[3] A. S. Al-Ezzi and M. N. M. Ansari, "Photovoltaic solar cells: a review," *Appl. Syst. Innov.*, vol. 5, no. 4, p. 67, 2022.

[4] W. Zhu, S. Wang, X. Zhang, A. Wang, C. Wu, and F. Hao, "Ion Migration in Organic–Inorganic Hybrid Perovskite Solar Cells: Current Understanding and Perspectives," *Small*, vol. 18, no. 15, p. 2105783, Apr. 2022, https://doi.org/10.1002/smll.202105783

[5] D. Devadiga, M. Selvakumar, P. Shetty, and M. S. Santosh, "Recent progress in dye sensitized solar cell materials and photo-supercapacitors: A review," *J. Power Sources*, vol. 493, p. 229698, 2021.

[6] A. Pallikkara and K. Ramakrishnan, "Efficient charge collection of photoanodes and light absorption of photosensitizers: A review," *Int. J. Energy Res.*, vol. 45, no. 2, pp. 1425–1448, Feb. 2021, https://doi.org/10.1002/er.5941

[7] A. Banerjee, "The design, fabrication, and photocatalytic utility of nanostructured semiconductors: focus on TiO_2-based nanostructures," *Nanotechnol. Sci. Appl.*, p. 35, Feb. 2011, https://doi.org/10.2147/NSA.S9040

[8] C. M. Maghanga, J. Jensen, G. A. Niklasson, C.-G. Granqvist, and M. Mwamburi, "Transparent and conducting TiO_2: Nb films made by sputter deposition: Application to spectrally selective solar reflectors," *Sol. Energy Mater. Sol. Cells*, vol. 94, no. 1, pp. 75–79, 2010.

[9] F. I. Chowdhury, T. Blaine, and A. B. Gougam, "Optical transmission enhancement of fluorine doped tin oxide (FTO) on glass for thin film photovoltaic applications," *Energy Procedia*, vol. 42, pp. 660–669, 2013.

[10] S. C. Dixon, D. O. Scanlon, C. J. Carmalt, and I. P. Parkin, "n-Type doped transparent conducting binary oxides: an overview," *J. Mater. Chem. C*, vol. 4, no. 29, pp. 6946–6961, 2016.

[11] V. W. Muramba, "Preparation and Characterization of Transparent and Conducting Doped Tin Oxide Films," PhD Thesis, Masters thesis, 2013.

[12] B. Li, L. Huang, M. Zhou, N. Ren, and B. Wu, "Surface morphology and photoelectric properties of fluorine-doped tin oxide thin films irradiated with 532 nm nanosecond laser," *Ceram. Int.*, vol. 40, no. 1, pp. 1627–1633, 2014.

[13] C.-Y. Tsay and S.-C. Liang, "Fabrication of p-type conductivity in SnO_2 thin films through Ga doping," *J. Alloys Compd.*, vol. 622, pp. 644–650, 2015.

[14] H. P. Dang, Q. H. Luc, V. H. Le, and T. Le, "The influence of deposition temperature and annealing temperature on Ga-doped SnO_2 films prepared by direct current magnetron sputtering," *J. Alloys Compd.*, vol. 687, pp. 1012–1020, Dec. 2016, https://doi.org/10.1016/j.jallcom.2016.06.236

[15] A. S. Ahmed, M. Shafeeq M., M. L. Singla, S. Tabassum, A. H. Naqvi, and A. Azam, "Band gap narrowing and fluorescence properties of nickel doped SnO_2 nanoparticles," *J. Lumin.*, vol. 131, no. 1, pp. 1–6, Jan. 2011, https://doi.org/10.1016/j.jlumin.2010.07.017

[16] Q. Jiang, X. Zhang, and J. You, "SnO_2 : A Wonderful Electron Transport Layer for Perovskite Solar Cells," *Small*, vol. 14, no. 31, p. 1801154, Aug. 2018, https://doi.org/10.1002/smll.201801154

[17] A. M. Ganose and D. O. Scanlon, "Band gap and work function tailoring of SnO_2 for improved transparent conducting ability in photovoltaics," *J. Mater. Chem. C*, vol. 4, no. 7, pp. 1467–1475, Feb. 2016, https://doi.org/10.1039/C5TC04089B

[18] S. Sujatha Lekshmy and K. Joy, "Structural and optoelectronic properties of indium doped SnO_2 thin films deposited by sol gel technique," *J. Mater. Sci. Mater. Electron.*, vol. 25, no. 4, pp. 1664–1672, Apr. 2014, https://doi.org/10.1007/s10854-014-1781-x

[19] K. Ravichandran and K. Thirumurugan, "Type inversion and certain physical properties of spray pyrolysed SnO_2: Al films for novel transparent electronics applications," *J. Mater. Sci. Technol.*, vol. 30, no. 2, pp. 97–102, 2014.

[20] S. Yu, W. Zhang, L. Li, D. Xu, H. Dong, and Y. Jin, "Fabrication of p-type SnO_2 films via pulsed laser deposition method by using Sb as dopant," *Appl. Surf. Sci.*, vol. 286, pp. 417–420, 2013.

[21] H. M. Ali and A. M. A. Hakeem, "Characterization of n and p-type (SnO_2) x (ZnO) 1-x nanoparticles thin films," *Eur. Phys. J. Appl. Phys.*, vol. 72, no. 1, p. 10301, 2015.

[22] Y. Li, R. Deng, Y. Tian, B. Yao, and T. Wu, "Role of donor-acceptor complexes and impurity band in stabilizing ferromagnetic order in Cu-doped SnO_2 thin films," *Appl. Phys. Lett.*, vol. 100, no. 17, 2012, Accessed: May 18, 2025. Available: https://pubs.aip.org/aip/apl/article/100/17/172402/385057

[23] S. S. Pan *et al.*, "p-type conduction in nitrogen-doped SnO_2 films grown by thermal processing of tin nitride films," *Appl. Phys. A*, vol. 109, no. 2, pp. 267–271, Nov. 2012, https://doi.org/10.1007/s00339-012-7288-5

[24] M.-H. Lee, Y.-C. Peng, and H.-C. Wu, "Effects of intrinsic defects on electronic structure and optical properties of Ga-doped ZnO," *J. Alloys Compd.*, vol. 616, pp. 122–127, 2014.

[25] K. Teshome, M. Birile, N. A. Tegegne, and F. G. Hone, "Effects of gallium doping on the structural, optical and electronic properties of PbS: Experimental and computational study," *Optik*, vol. 259, p. 168964, 2022.

[26] R. J. Deokate *et al.*, "Structural, optical and electrical properties of chemically sprayed nanosized gallium doped CdO thin films," *J. Alloys Compd.*, vol. 496, no. 1–2, pp. 357–363, 2010.

[27] J. Ungula, "Formation and characterization of novel nanostructured un-doped and Ga-doped ZnO transparent conducting thin films for photoelectrode," PhD Thesis, University of the Free State (Qwaqwa Campus), 2018. Accessed: May 18, 2025. Available: https://scholar.ufs.ac.za/items/ffba44e9-7e56-4501-96c6-53bba11e6504

[28] Z. Kaddachi, M. Belhi, R. Gharbi, and M. B. Karoui, "Effect of Ga doped TiO 2 photoanode on photovoltaic performances of natural dye-sensitized solar cells," in *2019 19th International Conference on Sciences and Techniques of Automatic Control and Computer Engineering (STA)*, IEEE, 2019, pp. 90–94. Accessed: May 18, 2025. Available: https://ieeexplore.ieee.org/abstract/document/8717275/

[29] A. Kaphle, *Cobalt Doped ZnO and CuO Nanomaterials for Photovoltaic Applications*. The University of Tulsa, 2019. Accessed: May 18, 2025. Available: https://search.proquest.com/openview/f96e03c60be6a9bdc38253e704ea5bde/1?pq-origsite=gscholar&cbl=18750&diss=y

[30] Y. Yuan *et al.*, "Toward emerging gallium oxide semiconductors: A roadmap," *Fundam. Res.*, vol. 1, no. 6, pp. 697–716, 2021.

[31] M. P. Subramaniam, G. Arunachalam, R. Kandasamy, P. Veluswamy, and I. Hiroya, "Effect of pH and annealing temperature on the properties of tin oxide nanoparticles prepared by sol–gel method," *J. Mater. Sci. Mater. Electron.*, vol. 29, no. 1, pp. 658–666, Jan. 2018, https://doi.org/10.1007/s10854-017-7959-2

[32] G. E. Patil, D. D. Kajale, V. B. Gaikwad, and G. H. Jain, "Preparation and characterization of SnO_2 nanoparticles by hydrothermal route," *Int. Nano Lett.*, vol. 2, no. 1, p. 17, July 2012, https://doi.org/10.1186/2228-5326-2-17

[33] F. Paraguay-Delgado *et al.*, "Structural analysis and growing mechanisms for long SnO_2 nanorods synthesized by spray pyrolysis," *Nanotechnology*, vol. 16, no. 6, p. 688, Mar. 2005, https://doi.org/10.1088/0957-4484/16/6/011

[34] S. V. Nagirnyak, V. A. Lutz, T. A. Dontsova, and I. M. Astrelin, "Synthesis and Characterization of Tin (IV) Oxide Obtained by Chemical Vapor Deposition Method," *Nanoscale Res. Lett.*, vol. 11, no. 1, p. 343, Dec. 2016, https://doi.org/10.1186/s11671-016-1547-x

[35] M. Kumar, A. Mehta, A. Mishra, J. Singh, M. Rawat, and S. Basu, "Biosynthesis of tin oxide nanoparticles using Psidium Guajava leave extract for photocatalytic dye degradation under sunlight," *Mater. Lett.*, vol. 215, pp. 121–124, Mar. 2018, https://doi.org/10.1016/j.matlet.2017.12.074

[36] F. K. Alsammarraie, W. Wang, P. Zhou, A. Mustapha, and M. Lin, "Green synthesis of silver nanoparticles using turmeric extracts and investigation of their antibacterial activities," *Colloids Surf. B Biointerfaces*, vol. 171, pp. 398–405, Nov. 2018, https://doi.org/10.1016/j.colsurfb.2018.07.059

[37] D. Horwat *et al.*, "Chemistry, phase formation, and catalytic activity of thin palladium-containing oxide films synthesized by plasma-assisted physical vapor deposition," *Surf. Coat. Technol.*, vol. 205, pp. S171–S177, July 2011, https://doi.org/10.1016/j.surfcoat.2010.12.021

[38] G. E. Hoag, J. B. Collins, J. L. Holcomb, J. R. Hoag, M. N. Nadagouda, and R. S. Varma, "Degradation of bromothymol blue by 'greener'nano-scale zero-valent iron synthesized using tea polyphenols," *J. Mater. Chem.*, vol. 19, no. 45, pp. 8671–8677, 2009.

[39] S. Ahmed and S. Ikram, "Silver nanoparticles: one pot green synthesis using Terminalia arjuna extract for biological application," *J Nanomed Nanotechnol*, vol. 6, no. 4, pp. 1–6, 2015.

[40] H. S. Devi, M. A. Boda, M. A. Shah, S. Parveen, and A. H. Wani, "Green synthesis of iron oxide nanoparticles using Platanus orientalis leaf extract for antifungal activity," *Green Process. Synth.*, vol. 8, no. 1, pp. 38–45, Jan. 2019, https://doi.org/10.1515/gps-2017-0145

[41] N. Kataria and V. K. Garg, "Green synthesis of Fe_3O_4 nanoparticles loaded sawdust carbon for cadmium (II) removal from water: Regeneration and mechanism," *Chemosphere*, vol. 208, pp. 818–828, Oct. 2018, https://doi.org/10.1016/j.chemosphere.2018.06.022

[42] I. H. Ifijen, E. U. Ikhuoria, S. O. Omorogbe, B. Anegbe, E. M. Jonathan, and D. I. Chikaodili, "Chemical, plant and microbial mediated synthesis of tin oxide nanoparticles: antimicrobial and anticancer potency," *Braz. J. Chem. Eng.*, vol. 40, no. 4, pp. 965–991, Dec. 2023, https://doi.org/10.1007/s43153-023-00315-0

[43] J. Jepngetich, S. A. Opiyo, P. W. Njoroge, and S. Kiprotich, "Effects of Ag Doping Concentrations on Structural and Optical Properties of Citrus Reticulata Capped ZnO Nanoparticles," 2025, Accessed: May 17, 2025. Available: https://doi.org/10.47363/jnsrr/2025(7)176

[44] S. Siyalo, H. F. Etefa, and F. B. Dejene, "Enhancing structural and optical properties of CuO thin films through gallium doping: A pathway to enhanced photoluminescence and predict for solar cells applications," *Chem. Phys. Impact*, vol. 10, p. 100832, June 2025, https://doi.org/10.1016/j.chphi.2025.100832

[45] H. Kafashan, Z. Orshesh, A. Bahrami, and F. Zakerian, "Structural and optoelectronic properties of electrodeposited CdSe thin films: effect of Cu-dopant," *Phys. B Condens. Matter*, vol. 675, p. 415623, 2024.

[46] S. S. Shinde, P. S. Shinde, Y. W. Oh, D. Haranath, C. H. Bhosale, and K. Y. Rajpure, "Structural, optoelectronic, luminescence and thermal properties of Ga-doped zinc oxide thin films," *Appl. Surf. Sci.*, vol. 258, no. 24, pp. 9969–9976, Oct. 2012, https://doi.org/10.1016/j.apsusc.2012.06.058

[47] H. Siddiqui, M. R. Parra, and F. Z. Haque, "Optimization of process parameters and its effect on structure and morphology of CuO nanoparticle synthesized via the sol- gel technique," *J. Sol-Gel Sci. Technol.*, vol. 87, pp. 125–135, 2018.

[48] G. S. Waweru, S. Kiprotich, and P. Waithaka, "Effects of growth temperature on the structural and optical properties of synthesized titanium dioxide nanoparticles," 2024, Accessed: May 16, 2025. Available: https://idl-bnc-idrc.dspacedirect.org/bitstreams/1e065307-334f-44fa-9559-d21854b73e9d/download

[49] K. Bett and S. Kiprotich, "Effects of Stirring Speed of Precursor Solution on the Structural Optical and Morphological Properties of ZnO Al Ga CoDoped Nanoparticles Synthesized via a Facile Sol Gel Technique," 2024, Accessed: May 07, 2025. Available: https://idl-bnc-idrc.dspacedirect.org/bitstreams/f20815b8-0713-4f7f-832b-de87cdf7d197/download

[50] M. Saha, S. Ghosh, V. D. Ashok, and S. K. De, "Carrier concentration dependent optical and electrical properties of Ga doped ZnO hexagonal nanocrystals," *Phys. Chem. Chem. Phys.*, vol. 17, no. 24, pp. 16067–16079, 2015, https://doi.org/10.1039/C4CP05480F

[51] E. T. Seid and F. B. Dejene, "Gallium and indium co-doping effects on structural, optical and luminescence properties of ZnO nanostructures," *Mater. Today Commun.*, vol. 27, p. 102330, 2021.

[52] B. Shanmuga Priya, M. Shanthi, C. Manoharan, and S. Dhanapandian, "Synthesis, characterization and photocatalytic activity of pure and Zn-doped In_2O_3 nanostructures," *J. Mater. Sci. Mater. Electron.*, vol. 28, no. 17, pp. 12784–12794, Sept. 2017, https://doi.org/10.1007/s10854-017-7106-0

[53] D. N. Papadimitriou, "Structural, optical, electrical properties, and strain/stress of electrochemically deposited highly doped ZnO layers and nanostructured ZnO antireflective coatings for cost-effective photovoltaic device technology," *Thin Solid Films*, vol. 605, pp. 215–231, 2016.

[54] A. Samavati *et al.*, "Structural, optical and electrical evolution of Al and Ga co-doped ZnO/SiO_2 /glass thin film: role of laser power density," *RSC Adv.*, vol. 7, no. 57, pp. 35858–35868, 2017, https://doi.org/10.1039/C7RA04963C

[55] H. J. Al-Asedy, A. A. Ati, N. Bidin, and S.-L. Lee, "Gallium contents-dependent improved behavior of sol–gel-grown Al: Ga co-doped ZnO nanostructures," *Appl. Phys. A*, vol. 123, no. 10, p. 665, Oct. 2017, https://doi.org/10.1007/s00339-017-1271-0

[56] N. S. Sabri, M. S. M. Deni, A. Zakaria, and M. K. Talari, "Effect of Mn Doping on Structural and Optical Properties of SnO_2 Nanoparticles Prepared by Mechanochemical Processing," *Phys. Procedia*, vol. 25, pp. 233–239, 2012, https://doi.org/10.1016/j.phpro.2012.03.077

[57] S. M. Hosseini, I. A. Sarsari, P. Kameli, and H. Salamati, "Effect of Ag doping on structural, optical, and photocatalytic properties of ZnO nanoparticles," *J. Alloys Compd.*, vol. 640, pp. 408–415, Aug. 2015, https://doi.org/10.1016/j.jallcom.2015.03.136

[58] N. Zebbar *et al.*, *Thin Solid Films*, vol. 605, pp. 89–94, 2016.

[59] M. Bhatnagar, V. Kaushik, A. Kaushal, M. Singh, and B. R. Mehta, "Structural and photoluminescence properties of tin oxide and tin oxide: C core–shell and alloy nanoparticles synthesised using gas phase technique," *AIP Adv.*, vol. 6, no. 9, 2016, Accessed: May 22, 2025. Available: https://pubs.aip.org/aip/adv/article/6/9/095321/884807

[60] D. P. Pham *et al.*, "In and Ga Codoped ZnO Film as a Front Electrode for Thin Film Silicon Solar Cells," *Adv. Condens. Matter Phys.*, vol. 2014, pp. 1–7, 2014, https://doi.org/10.1155/2014/971528

[61] H. Nasir *et al.*, "Variations in structural, optical, and dielectric properties of CuO nanostructures with thermal decomposition," *J. Mater. Sci. Mater. Electron.*, vol. 31, pp. 10649–10656, 2020.